JOURNAL OF MATERIALS SCIENCE 14 (1979) 800–810

An X-ray double crystal topographic assessment of defects in quartz resonators

K. L. BYE, R. S. COSIER
Philips Research Laboratories, Redhill, Surrey, UK

This paper describes an X-ray double crystal topographic study of defects in eighteen quartz resonators designed to operate at 1.4 MHz. The types of defects found in quartz are described, together with their reported effects on resonator performance. The mode of operation of the bulk resonator and the technique of X-ray double crystal reflection topography are outlined. Topographs reveal the electrode structures and surface features of the resonators together with the presence of growth defects such as dislocation cells, sub-boundaries, growth striations and growth sector boundaries. Spurious flexure modes in two resonators are also shown. It is demonstrated that a correlation exists between the presence of growth striations (and probably sub-boundaries) and a higher equivalent series resistance of the resonators. It is shown that such defects change the contributions to the losses, possibly by changing the nature of the vibration pattern of the resonator.

1. Introduction

The AT-cut (referring to a particular orientation) bulk quartz resonator is widely used for frequency control and selection, since it has a low temperature coefficient of frequency and high quality factor. Such resonators are manufactured by Cathodeon Crystals, Ltd, Linton, Cambridge, using synthetic quartz from a variety of sources. This paper describes our investigation by X-ray double crystal reflection topography of 18 of these resonators (designed to operate at 1.4 MHz) to see if any features we observed could be correlated with the performance of the resonators.

Section 2 reviews the hydrothermal growth of synthetic quartz, the defects present in the crystals and their reported effect on the performance of resonators. The mode of operation of the bulk resonator is outlined in Section 3, while the experimental arrangement for the X-ray double crystal reflection topography is described in Section 4. Topographs (Section 5) reveal the electrode structures and surface features of the resonators together with the presence of growth defects such as dislocation cells, sub-boundaries, growth striations and growth sector boundaries. Spurious flexure modes on two resonators are also shown. It is demonstrated that a correlation exists between the presence of growth striations (and probably sub-boundaries) and a higher equivalent series resistance of the resonator. A summary of the effects of flexure modes and individual defects on the equivalent series resistance is given in Section 6. Finally, it is shown that the deleterious defects change the external contributions to the losses, possibly by changing the nature of the vibration pattern of the resonator.

2. Synthetic quartz crystals

Synthetic quartz is grown by conventional hydrothermal techniques [1–3] using autoclaves capable of operating at high temperatures and pressures. Conditions are such that dissolution occurs in one chamber, transport of the solute then takes place by convection through a baffle into an isothermal chamber, where recrystallization onto the seed crystal occurs. Growth rates depend on such factors as the seed orientation, growth direction, the solvent used for transport, temperature and pressure. Generally the slower the growth rate the fewer the impurities present. It has been shown [4, 5] that material from the Z-growth sectors (Fig. 1) has the lowest impurity content. Hence, for Y-cut or AT-cut quartz crystal resonators, Y-plates are used for the seed (Fig. 1). The AT-cut

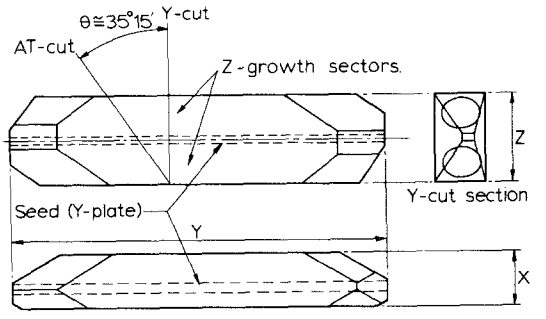

Figure 1 A *Y*-bar of synthetic quartz showing the orientations of the *Y*-cut and AT-cut plates.

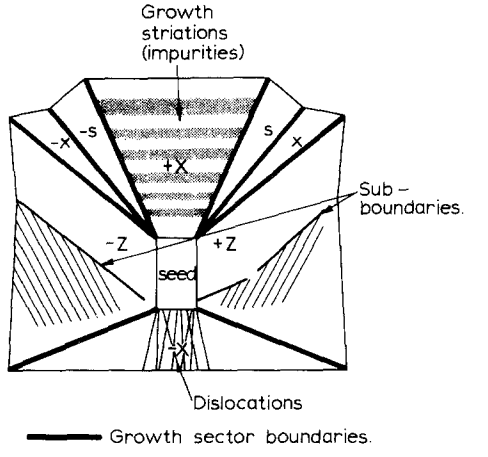

Figure 2 Schematic illustration of growth sectors, dislocations, growth striations and sub-boundaries in a *Y*-cut plate of quartz.

is similar to the *Y*-cut but involves an additional rotation of 35° 15′ around the *X*-axis. Hence, growth features found on *Y*-cut plates will also be found on AT-cut plates. Fig. 2 shows that during growth onto the *Y*-plate seed, various types of lattice distortion and imperfection may occur. Four major growth sectors $\pm X$, $\pm Z$, surround the seed together with the *x* and *s* minor growth sectors. Recently it has been shown [6] that the boundary between the $-X$ and *Z* growth sectors is coherent. Differences in the unit cell dimensions in these sectors were also reported. Each growth sector has a distinctive pattern of imperfections. Defects such as dislocations, sub-boundaries and growth striations are often present in the different growth sectors.

2.1. Dislocations

Dislocations due to poor epitaxy on the seed have been observed [7–9] in the $\pm X$ and $\pm Z$ growth sectors. They have a tendency to fan out from the seed crystal, making a maximum angle with the $\pm X$- or $\pm Z$- axes of about 30°. The density of dislocations has been found to be lower for slower rates of growth [7]. Few dislocations nucleate in the volume of the crystal away from the seed [8]. As a result of the strain field around dislocations, they usually act as sinks for suitable impurities, interstitials and vacancies [10]. The predominant decorating species is probably OH [11]. The dislocations in natural quartz usually exhibit contortions due to impurities [12]. However, Lang and Miuscov [8] found this was not the case for the Z growth sector dislocations in their own synthetic quartz. It was also found [8] that at higher dislocation densities (3×10^3 lines cm^{-2}) a cellular growth develops in the *Z*-direction as growth proceeds. The cell walls were identified as fault surfaces which outcropped in the grooves of the cobbled *Z*-face. It has been suggested [13] that this cobbled surface arises because of the slower growth rate at the cell walls caused by a high concentration of impurity associated with the edge dislocations in the cell walls. However, the cobblestone *Z*-surface also occurs in low dislocation density crystals [11]. It is more likely that the strain due to the cell walls is relieved by the dislocations so that they collect preferentially in the walls [11]. McLaren *et al.* [13] have also observed very high dislocation densities in two quartz plates with abnormally large hydrogen concentrations (>5000 ppm Si). This has been explained by Griggs [14] who has shown that dislocations are more mobile in the presence of hydrogen and hence are able to multiply.

Since dislocations often have impurities associated with them it is difficult to assess the effects of dislocations alone on the acoustic loss of a resonator. It has been reported [7] that at dislocation densities of 10^3 to 10^4 lines cm^{-2} the *Q* of a 5 MHz resonator was reduced by a factor of twenty compared with a low dislocation density resonator (10 to 10^2 lines cm^{-2}). For dislocation densities less than about 10^2 lines cm^{-2}, no significant contributions to the room temperature acoustic loss have been found [9, 15]. Since it is now possible to grow essentially dislocation-free quartz crystals routinely [9, 15] this problem in the manufacture of quartz resonators should no longer exist.

2.2. Sub-boundary (SB)

In essentially dislocation-free quartz crystals, an additional feature has been observed in the $\pm Z$

growth sectors. To distinguish it from the other growth sector boundaries (Fig. 2) it has been called a sub-boundary [9, 16]. This sub-boundary can usually be traced from close to the $-X$ end of the seed crystal, extending approximately parallel to the $-Z/-x$ and the $+Z/+x$ growth sector boundaries in the $-Z$ and $+Z$ growth sectors respectively. Associated with this sub-boundary a series of branches have been found [16], showing as weak contrast, which run back towards the $-X$ growth sector. The arrival point of some of these branches on the Z-face coincided with the grooves between the cobbles. The external features were also modified where the sub-boundary emerged on the Z-face. It has also been demonstrated by an infra-red scan across such a sub-boundary [9] that the concentration of OH is higher in the vicinity of the sub-boundary compared with that in the normal $\pm Z$ growth sectors. The X-ray topographic contrast of the sub-boundary has been shown [16] to be due to local lattice dilation. It is suggested that local stresses and strains existing in the crystal due to the difference in lattice spacing of the different growth sectors cause the impurity localization along the sub-boundary faces.

Measurements have been reported [9] of the Q, equivalent series resistance, inflection temperature and first-order temperature coefficient of AT-cut flat-parallel quartz resonators at frequencies of 24, 40, 56, 72 and 88 MHz. The presence of a sub-boundary had no significant effect on these electrical characteristics.

2.3. Impurities

Hydrogen, often in the form of OH, is the major impurity in synthetic quartz crystals. It is detected by an infra-red absorption band and by the effect it has on the acoustic loss of resonators [15, 17]. Defect models accounting for the known properties have been suggested [15, 18, 19], but only the model involving hydrolized bonds [18] can account for all of the OH found [11]. It has been demonstrated [17, 20, 21] that the acoustic loss increases with the OH concentration. It was found that the large loss peak around 100° C was related to the OH concentration, and that the room temperature acoustic loss was due to the stretching of the OH bond.

Variations of the refractive index along planes perpendicular to the growth direction have been reported [22]. Subsequent infra-red measurements [20, 21] demonstrated that they were caused by variations in the OH concentration. Similar growth striations are often observed X-ray topographically in all the growth sectors of the Y-cut plate (Fig. 2). They are usually caused by lattice parameter variations associated with the changes in the impurity segregation as the growth rate changes.

The other major impurities found in synthetic quartz are the alkali ions (sodium, lithium and potassium) and aluminium. The alkali ions all exhibit characteristic losses [15] both below and above room temperature. Aluminium which appears to enter the lattice as a substitutional Al^{3+} associated with a charge compensating interstitial ion (Na^+, Li^+, K^+) also contributes to losses below and above room temperature.

Since hydrogen (probably in the form of hydrolized bonds) remains the most significant contributor to the room temperature acoustic loss, care must be taken to ensure that as little as possible is incorporated during growth. The incorporation of ions such as Al and Fe leads to higher OH content. Fast growth also leads to a high OH content. Concentrations of OH as high as 7000 ppm SiO_2 have been reported [15]. However, provided care is taken to reduce the impurity content and ensure slow growth rates, the OH concentration can be reduced to below 1000 ppm and the quality factor (Q) of approximately 2×10^6 may be obtained [9, 11].

2.4. Growth sector boundaries (GSB)

Wilson [23] reported that growth sector boundaries affected the temperature coefficient of frequency of bulk quartz resonators. He suggested that the different elastic properties of the different sectors and/or the impurity concentration at the growth sector boundaries caused the electrical loss at higher frequencies. More recently, similar effects were reported by Parpia [24] who observed deviations from the ideal in the frequency–temperature behaviours of quartz resonators with growth sector boundaries present. He investigated twenty 12 mm diameter AT-cut quartz resonators with a 7 MHz fundamental frequency. It was suggested that changes in the frequency–temperature characteristics may be due to either the nature of the boundaries themselves or the different impurity concentration in the vibrating region.

3. Bulk resonators

The AT-cut quartz resonator is the most widely used in frequency control and selection because of

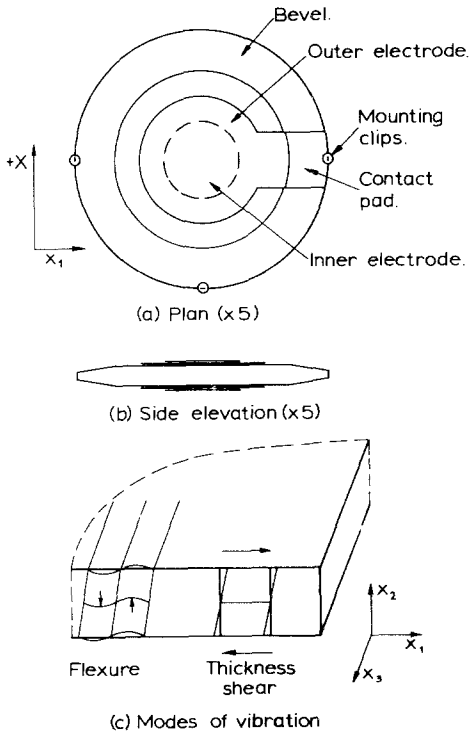

Figure 3 (a) and (b) 1.4 MHz AT-cut quartz resonator. (c) Resonance modes.

its small temperature coefficient and large quality factor (Q). Fig. 3a and b shows the appearance of a resonator designed to operate at about 1.4 MHz (thickness = 1.2 mm). The circular AT-cut plate is bevelled in order to prevent energy reaching the edge. Electrical contact to a pair of silver outer electrodes is made via the contact pads, conducting cement and mounting clips. The inner electrodes are evaporated towards the end of the processing in order to trim the frequency to the desired value. The physical characteristics (e.g. thickness, diameter, bevel, electrode weights, etc.) of these resonators have been designed to ensure that when suitably driven they vibrate in a fundamental thickness shear mode [25, 26]. The displacements associated with such a thickness shear mode and a flexure mode are illustrated in Fig. 3c. For the thickness shear mode displacements are parallel to the plane of the plate while for flexure modes they are perpendicular to this plate. In the real crystal resonator (Fig. 3a) the direction of the thickness shear displacement (x_1) is shown to be perpendicular to the $+X$ direction. As a result of strain or changes of temperature, unwanted flexural and shear modes are sometimes introduced. These modes can degrade the performance of the resonator [23].

4. Double crystal topography

Double crystal reflection X-ray topography is a fairly quick, non-destructive technique for observing surface defects and strain or growth defects such as dislocations, growth striations, growth sector boundaries, stacking faults and twins [24, 28]. Areas of a few cm^2 may be assessed in a single topograph providing good quality crystals are used. These factors, combined with an optimum resolution of a few microns, makes this technique ideal for investigating defects in quartz resonators.

Fig. 4 shows a schematic diagram of a double crystal diffractometer in the (+ −) setting. Asymmetric diffraction of the X-ray beam from a point source by a perfect reference crystal produces a beam with broad lateral coherence and a very small angular divergence. For the 1 1 5 reflection from a (1 1 1) silicon slice using Cu$K\alpha$ radiation the divergence is less than 1 arc second. Further diffraction by the sample, set close to the Bragg angle (θ_B), results in an image of the crystal defects being formed on the film. If the sample is slowly rotated through the Bragg condition and the diffracted intensity plotted as a function of θ then a rocking curve is obtained (Fig. 4). For the 0 4 $\bar{1}$ reflection from quartz, the half width of this rocking curve is only a few seconds since the interplanar spacing matches that for the (1 1 5) reference crystal reflection. Optimum sensitivity for topographs is obtained by setting the sample crystal to diffract at half the maximum intensity. For quartz crystals a 10% change in intensity on topographs is caused

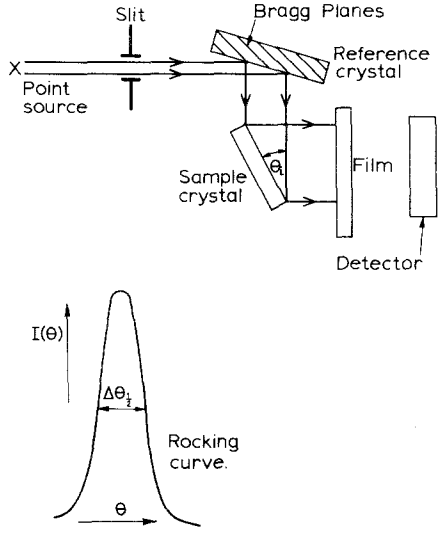

Figure 4 Schematic diagram of the double crystal diffractometer and the associated rocking curve.

by a misorientation from the Bragg angle of only a few tenths of a second. As a consequence of such a narrow rocking curve, the contrast of dislocations, sub-grains and stacking faults is due to homogeneous dilation and tilt [29].

Throughout these investigations the $0\,4\,\bar{1}$ reflection was used, for which $\theta_i = 23.4^\circ$ (Fig. 4) and $\theta_B = 47.6^\circ$. The penetration depends on the quality of the crystals but varies from about 15 μm for a perfect crystal to about 70 μm for an imperfect one. The typical exposure time for topographs was $\frac{1}{2}$ h. In order to observe any unwanted flexure modes (Section 3) a series of topographs was also taken while resonators were being driven. When a perfect crystal is sufficiently distorted by an acoustic resonance the diffracted intensity of a particular Bragg reflection increases to that predicted by the kinematical theory [27]. Hence topographs taken while the quartz platelet is being driven at its resonant frequency will show contrast due to any suitable resonant modes. It has been shown [30, 31] that the diffracted intensity is only sensitive to modes with a displacement normal to the Bragg planes, with either a bending distortion in the plane of the incident and diffracted wave vectors or those giving rise to a change in lattice spacing. With reflection topography it is only possible to use Bragg planes which are not more than about 30° from the plane of the plate. Since only displacements normal to the Bragg planes produces any contrast, it follows that only flexure modes will give strong contrast while that due to the thickness shear modes will be very weak. Topographs will not show contrast due to the fundamental shear mode.

5. Results

5.1. Topographs of the resonators

Topographs of five of the eighteen AT-cut quartz resonators are shown in Fig. 5a to e. These topographs illustrate the principal features observed on all eighteen resonators. The $+X$ direction is vertical. All show some contrast effects due to the electrode structures and mounting clips but these are most clearly seen in Fig. 5c. The positions of the mounting clips (m), the circular edge of the bevel (b), the outer electrode (o) and the inner electrode (i) are evident.

Six resonators showed well-defined features such as those in Fig. 5a, which are consistent with the presence of a dislocation network (white lines are dislocations) which has developed the cellular structure described by Lang [8] (Section 2.1). The density of dislocations is approximately 10^2 to 10^3 lines cm^{-2}. They were generally found on those resonators cut from the Z growth sector, with no growth sector boundaries present.

Five resonators were found to have a prominant sub-boundary, three in the $+Z$ growth sector, e.g. Fig. 5b, and the other two in the $-Z$ growth sector, e.g. Fig. 5e. The line of the sub-boundary runs approximately parallel to the $+Z/x$ or $-Z/-x$ growth sector boundaries. Although all the sub-boundaries are pointing back towards where the $-X$ end of the seed crystal used to be (Fig. 2), contrast is lost about 2 to 5 mm from the resonator edge. All the resonators with sub-boundaries have either $+Z/-X$ and $+Z/+x$ growth boundaries or $-Z/-X$ and $-Z/-x$ growth sector boundaries. Few dislocations are evident but growth striations can often be seen in the Z growth sectors (e.g. Fig. 5e). The branches described by Yoshimura and Kohra [16] as running back from the sub-boundary towards the $-X$ growth sector (Fig. 2) are only clearly visible in Fig. 5e. However, they are larger and not as regular as those reported earlier [16].

Growth striations caused by changes in the impurity content of the crystal, were observed in nine resonators. The four resonators with fairly prominent growth striations are shown in Fig. 5b to e. Three of these (b, d and e) have growth sector boundaries. The pitch of the striations is approximately 100 μm while their direction is normal to the direction of growth.

5.2. Topographs of spurious flexure modes

As described in Section 3, the resonators were designed to resonate in their fundamental shear mode. However, in order to see if any unwanted flexure modes were present, double crystal reflection topographs were taken while the resonator was being driven with the fundamental frequency of the resonator (1.4 MHz). The two resonators which showed these unwanted flexure modes are shown in Fig. 6a and b. Contrast due to these flexure vibrations is evident near the centre of the resonators.

5.3. Equivalent series resistance and defects

The quality factor, Q, of a resonator is related to the equivalent series resistance (ESR) by the

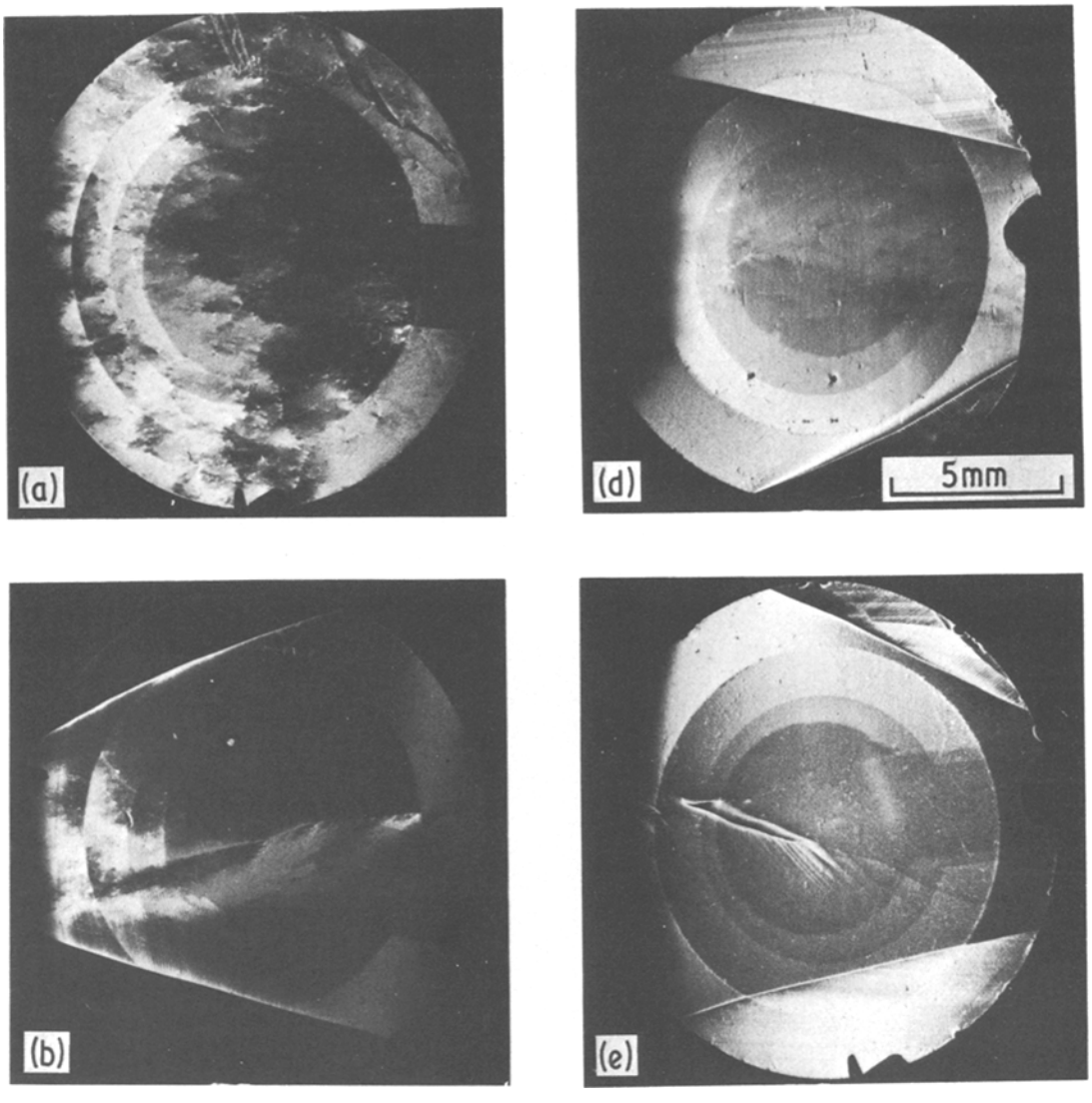

Figure 5 Double crystal reflection topographs of quartz resonators. See Section 5.1 for details.

expression:

$$Q = \frac{\omega L}{ESR}$$

where L is inductance, and $\omega = 2\pi \times$ resonant frequency. Measurements were made using a phase-locked π network.

In order to see if there was any correlation at all between the presence of sub-boundaries, growth striations, cobblestones or the presence of additional growth sectors, a graph of ESR versus the number of defects was plotted (Fig. 7).

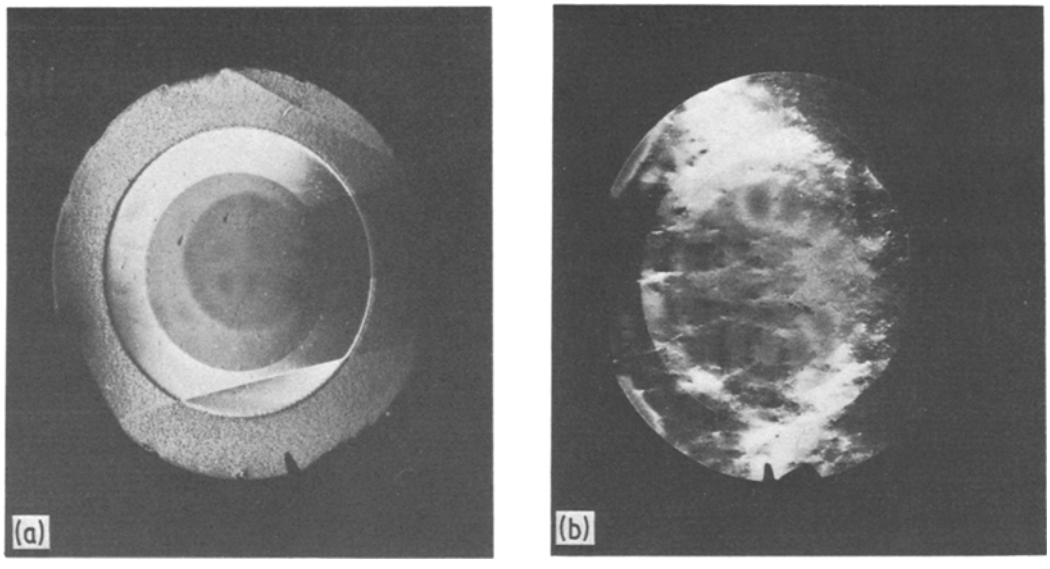

Figure 6 Double crystal reflection topographs showing spurious resonant modes in the central regions of two quartz resonators.

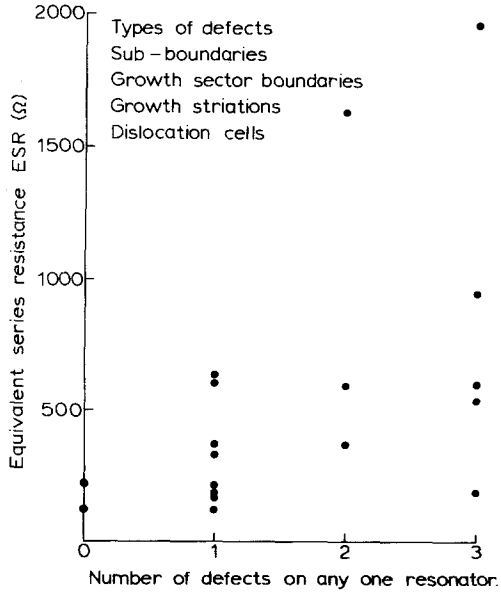

Figure 7 Equivalent series resistance dependence on the number of defects observed in any one resonator.

Although there is considerable spread in ESR perhaps due to other parameters such as mounting strain, surface finish, electrode structures, etc., Fig. 7 shows that, generally, resonators with the lowest ESR are those with the fewer growth defects.

The analysis has been carried further in Table I which lists the growth defects present in the eight-een resonators which have themselves been listed in order of ascending ESR. A tick indicates the presence of that particular defect in the resonator. Rocking curve half widths are also listed. The series has been divided into two halves by the line ab. Generally, a defect which tends to increase the ESR should have more ticks below ab than above. This is the case for the sub-boundary where only one of the nine resonators with the lowest ESR has this defect compared with four of those with the highest ESR. For dislocation cells there are three above ab and three below ab, suggesting that they had little influence on the ESR. The two resonators with spurious flexure modes both had a low ESR (Section 6.1). For resonators with growth striations two lie above ab and seven below. This suggests that growth striations are associated with a higher ESR. Finally, for growth sector boundaries there are three above ab and six below. However, growth sector boundaries are often present with either a sub-boundary (5) or growth striations (7), both of which are associated with a higher ESR. The fact that the two resonators with only growth sector boundaries have relatively low ESRs (124 and 202 Ω) suggests that the presence of these boundaries does not increase the ESR (Section 6.3).

The Mann–Whitney U test (see Appendix) has been applied to test statistically the significance of the effects of the various growth defects on the

TABLE I

Resonator no.	ESR (Ω)	Sub-boundary	Dislocation cells	Spurious modes (flexure)	Growth striations	Growth sector boundaries	Half width (sec)
1	124	×	×	√	×	√	5.0
2	133	×	×	×	×	×	6.5
3	194	√	×	×	√w*	√	4.0
4	202	×	×	×	×	√	8.8
5	209	×	√	√	×	×	9.8
6	213	×	×	×	×	×	8.3
7 (Fig. 5c)	219	×	×	×	√	×	3.5
8	333	×	√	×	×	×	6.1
9	375	×	√	×	×	×	8.8
10	375	×	×	×	√w	√	8.6
11	540	√	×	×	√w	√	5.8
12 (Fig. 5d)	600	×	×	×	√	√	6.1
13 (Fig. 5a)	607	×	√	×	×	×	6.1
14 (Fig. 5b)	607	√	×	×	√	√	8.1
15	641	×	√	×	×	×	12.1
16	955	√	×	×	√w	√	5.5
17	1641	×	√	×	√w	×	7.8
18 (Fig. 5e)	1975	√	×	×	√	√	4.0
No. of ticks above ab		1	3	2	2	3	
No. of ticks below ab		4	3	0	7	6	
U_T		18	26	3	18	37	
U		12	14	1	17	17	

a b

*w = weak striations.

TABLE II

Defects present or absent	Number of resonators	Average ESR (Ω)	Standard deviation (Ω)
Without growth striations or sub-boundary	9	320	180
With growth striations but without sub-boundary	4	710	560
With growth striations and sub-boundary	5	850	610
With only a GSB	2	163	40

ESR. To calculate U_T (Table I) the number of ticks preceding the crosses have been counted (except for spurious modes where the number of crosses preceding the ticks has been counted as there are more ticks above ab than below). The value of U is given in the Appendix. If $U_T < U$ then the probability of the occurrence of these results by chance is less than 5%. This is not the case for any defect, however, for growth striations $U_T = 18$ and $U = 17$. It follows that the probability that the growth striations are associated with a high ESR is a little less than 95%.

A comparison of the average ESR of resonators with and without some defects is shown in Table II. The average ESR of resonators with growth striations but without a sub-boundary is just over twice that for resonators with neither of these defects. When both growth striations and a sub-boundary are present this factor increases to × 2.7. Thus the ESR of a resonator with an isolated sub-boundary would be just under one and a half times that of a resonator with no such defect.

6. Discussion

The possible effects on the ESR of the 1.4 MHz resonators of each of the defects in turn will be considered, together with some comments on the presence of spurious resonance modes.

6.1. Spurious resonance modes

Both resonators showing contrast due to unwanted flexure modes had a low ESR. However, care must be exercised here since the contrast was poor and other weaker flexure modes may have been present in some other resonators. Moreover, unwanted shear modes are not detected by reflection topo-

graphy. For a comprehensive study of spurious modes, Lang transmission topography and double crystal reflection topography should be used. Using Lang topography, Wilson [23] reported that flexural modes increased the ESR and that such modes were related to the presence of activity dips. In general, spurious modes can lead to a decrease in Q (increased ESR) since energy may be lost through the mounts if the form of the modes is appropriate.

6.2. Dislocation cells

Dislocation cells were generally observed on those resonators cut from the pure Z growth sector, with no growth sector boundaries present. Typical densities were approximately 10^2 to 10^3 lines cm^{-2}. The presence of such dislocations had no significant effect on the ESR. This is consistent with previous investigations described earlier (Section 2.1).

6.3. Growth sector boundaries (GSB)

The presence of growth sector boundaries near the outside of the resonator was found to have no effect on the ESR of the resonators. However, the area of the additional growth sectors on the non-Z side of the GSBs was always less than about 10% of the total resonator area. In addition, the GSBs were always near the edge of the resonator where the energy of the mode is low. Hence it should not be concluded that a GSB across the middle of the resonator would not affect the ESR. Earlier investigators [23, 24] (Section 2.4) found that the presence of such growth sector boundaries in AT-cut quartz resonators affected the temperature dependence of the frequency. The different elastic properties of the different growth sectors due to changes in the impurity incorporation or the nature of the growth sector boundary itself are likely causes of these deleterious effects.

6.4. Growth striations

It has been found that the presence of growth striations on topographs of the resonators is associated with a higher ESR than those without such features. The magnitude of this change is approximately a factor of 2 (Section 5.3). Since growth striations are caused by periodic changes in the impurity concentration, the question arises as to what impurity is responsible. One possibility is OH (Section 2.3), since this can be incorporated in a periodic fashion. This impurity is particularly attractive at first sight since it is well known that high concentrations of OH are associated with a low Q (high ESR).

6.5. Sub-boundary

The situation for the sub-boundary is less well defined. Although statistically (95% confidence level) the presence of a sub-boundary has not been directly linked with a higher ESR, evidence has been presented to suggest that this may be the case. Firstly, only one of the nine resonators with the lowest ESR had this particular defect, while four of the nine with the highest ESR had this defect. Secondly, the average ESR of resonators with an isolated sub-boundary was calculated to be approximately 1.4 times the value for resonators without this defect. Studies by earlier investigators (Section 2.2) found that the presence of a sub-boundary did not significantly affect the electrical characteristics of resonators operating at frequencies from 24 to 88 MHz.

It has been reported previously (Section 2.2) that the local concentration of OH is higher in the region of the sub-boundary. Since the presence of high OH content is related to a low material Q (high ESR) it seems reasonable to link the low device Q (high ESR) with the high OH content. This is discussed below in Section 6.6.

6.6. Loss mechanisms

A large difference between the material Q and the final device Q is a common feature of quartz resonators. Warner [32] reported that the following factors have the effect of decreasing the Q:

(1) electrodes;

(2) spurious modes or a badly designed fundamental mode couples energy out via the mounts;

(3) surface finish – not important at low frequencies;

(4) air damping.

These factors account for the low device Q. The final overall quality factor (Q_T) is related approximately to the material Q (Q_0) and the external contributions listed above (Q_i) by an equation of the form:

$$\frac{1}{Q_T} = \frac{1}{Q_0} + \sum_i \frac{1}{Q_i} \qquad (1)$$

Substituting $Q_T = 4 \times 10^4$ for quartz resonators with no defects (material $Q = Q_0$) and also $Q_T = 2 \times 10^4$ for resonators with a defect

(material $Q = Q_D$), two equations are obtained:

$$\frac{1}{4 \times 10^4} = \frac{1}{Q_0} + \sum_i \frac{1}{Q_i} \quad (2)$$

and

$$\frac{1}{2 \times 10^4} = \frac{1}{Q_D} + \sum_i \frac{1}{Q_i} \quad (3)$$

If one assumes that the external contribution to the losses $[\sum_i (1/Q_i)]$ are the same for both cases, substitution in Equation 2 leads to the expression:

$$\frac{1}{Q_D} - \frac{1}{Q_0} = \frac{1}{4 \times 10^4} \quad (4)$$

A typical figure for the quality factor of free quartz is $Q_0 = 10^6$. Substituting in Equation 4 one obtains $Q_D = 3.8 \times 10^4$ as the material quality factor for the typical quartz resonator with a defect.

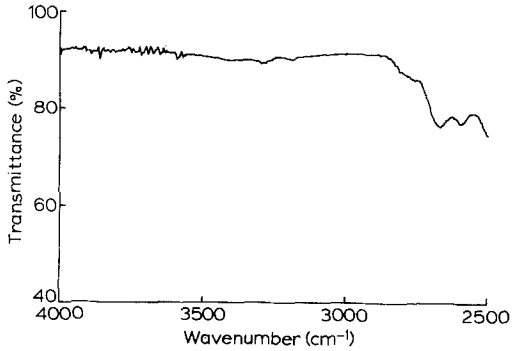

Figure 8 Variation of the transmittance with wave number of a quartz resonator with growth striations (Fig. 5d) and with the electrodes removed. Beam diameter = 7 mm. Crystal thickness = 1.2 mm.

It is also possible to calculate the material Q from the infra-red transmittance characteristics [11, 21]. Fig. 8 shows the wavenumber dependence of the transmittance of a polished quartz resonator with growth striations and with the electrodes removed. A small absorption band around 3590 cm^{-1} is evident. The material quality factor Q_D associated with this band is $>10^6$. Since the value of Q_D obtained using Equation 4 does not agree with this, it follows that Equation 4 is not valid. Hence the assumption that the external contributions to the losses $[\Sigma (1/Q_i)]$ were the same in both cases, is invalid. Conversely, this implies that the presence of the defects changes the external contributions to the losses.

Fletcher [33] suggests that the presence of defects such as the growth striations and the sub-boundaries may enhance the excitation of spurious modes due to the local variation in symmetry giving additional piezoelectric or elastic coefficients. With suitable modes, energy would be coupled out via the mounts, resulting in a lower Q. However, no contrast due to flexure modes was observed on any of the resonators with growth striations or sub-boundaries, although shear modes could not be detected. A further possibility is that these defects act as scattering centres for the fundamental mode. This mode is then spread out so that it overlaps the edges of the plate and energy is coupled out via the mounts. This could be checked by observing the fundamental mode using Lang topography. Clearly a rather more detailed investigation will be needed to resolve these questions.

7. Conclusions

X-ray double crystal reflection topography has proved to be a powerful technique for the rapid ($\frac{1}{2}$ h exposure time) observation of growth defects and spurious flexure modes in 1.4 MHz quartz resonators. A correlation has been found between the presence of growth striations (and probably sub-boundaries) and a higher equivalent series resistance of the resonators.

It has been shown that the presence of such defects change the external contributions to the losses, possibly by changing the nature of the vibration pattern of the resonator.

Appendix

Critical values of U at the 5% level

Should you wish to use the Mann–Whitney U test on groups which do not have ten numbers each, you should carry out the same ranking procedure and, having calculated U, enter the following table – where n_1 = the number in the smaller sample and n_2 = the number in the larger sample. If the value of U obtained is less than or equal to the value given in the table the probability of the occurrence of these results due to chance is 5% or less.

n_1	n_2											
	9	10	11	12	13	14	15	16	17	18	19	20
1												
2	0	0	0	1	1	1	1	1	2	2	2	2
3	2	3	3	4	4	5	5	6	6	7	7	8
4	4	5	6	7	8	9	10	11	11	12	13	13
5	7	8	9	11	12	13	14	15	17	18	19	20
6	10	11	13	14	16	17	19	21	22	24	25	27
7	12	14	16	18	20	22	24	26	28	30	32	34
8	15	17	19	22	24	26	29	31	34	36	38	41
9	17	20	23	26	28	31	34	37	39	42	45	48
10	20	23	26	29	33	36	39	42	45	48	52	55
11	23	26	30	33	37	40	44	47	51	55	58	62
12	26	29	33	37	41	45	49	53	57	61	65	69
13	28	33	37	41	45	50	54	59	63	67	72	76
14	31	36	40	45	50	55	59	64	67	74	78	83
15	34	39	44	49	54	59	64	70	75	80	85	90
16	37	42	47	53	59	64	70	75	81	86	92	98
17	39	45	51	57	63	67	75	81	87	93	99	105
18	42	48	55	61	67	74	80	86	93	99	106	112
19	45	52	58	65	72	78	85	92	99	106	113	119
20	48	55	62	69	76	83	90	98	105	112	119	127

Reproduced by kind permission of the Open University from *Biological Basis of Behaviour* (SDT 286 HEN).

Acknowledgements

We wish to thank Cathodeon Crystals, Ltd, for supplying the resonators and for loss measurements and W. S. Metcalf for his support. We also wish to thank Dr P. T. Greene, Dr E. D. Fletcher and Dr J. C. Brice for many useful discussions. Finally, we thank the PRL Photographic Department and Drawing Office for preparing the photographs and diagrams.

References

1. R. A. LAUDISE and R. A. SULLIVAN, *Chem. Eng. Prog.* **55** (1959) 55.
2. A. A. BALLMAN and R. S. LAUDISE, "The Art of Growing Crystals", (Wiley, New York, 1963) p. 231.
3. J. C. BRICE, *Rep. Prog. Phys.* **40** (1977) 567.
4. F. AUGUSTINE and D. R. HALE, *J. Chem. Phys.* **29** (1958) 685.
5. A. J. COHEN, *Phys. Chem. Solids* **13** (1960) 321.
6. D. Y. PARPIA, *Phil. Mag.* **33** (1976) 715.
7. W. J. SPENCER and K. J. HARUTA, *J. Appl. Phys.* **37** (1966) 549.
8. A. R. LANG and V. F. MIUSCOV, *ibid* **38** (1967) 2477.
9. J. ASAHARA, K. TAKAZAWA and H. VAZAKI, Proceedings of the 28th Annual Symposium on Frequency Control (1974) p. 117.
10. A. H. COTTRELL, "Dislocations and Plastic Flow in Crystals" (Oxford University Press, London, 1953).
11. J. C. BRICE, private communication.
12. A. R. LANG and V. F. MIUSCOV, *Acta. Cryst.* **20** (1966) A275.
13. A. C. MCLAREN, C. F. OSBORNE and L. A. SAUNDERS, *Phys. Stat. Sol.* **4** (1971) 235.
14. D. GRIGGS, *J. Geophys. Res.* **79** (1974) 1655.
15. B. F. FRASER, "Physical Acoustics" (Academic Press, New York and London, 1968) p. 59.
16. J. YOSHIMURA and K. KOHRA, *J. Crystal Growth* **33** (1976) 311.
17. D. M. DODD and D. B. FRASER, *J. Phys. Chem. Solids* **26** (1965) 673.
18. G. O. BRUNNER, H. WONDRATSCHEK and F. LAVES, *Z. Elektrochem.* **65** (1961) 735.
19. A. KATS, *Philips Res. Rept.* **17** (1962) 133.
20. D. B. FRASER, Symposium on Sonics Ultrasonics, Santa Monica, California (1964).
21. D. B. FRASER, 5th International Congress on Acoustics, Liege (1965).
22. G. W. ARNOLD, 11th Practical Annual Symposium on Frequency Control, SCEL, Fort Monmouth, New Jersey (1957) p. 112.
23. C. J. WILSON, Thesis, Cavendish Labs., Cambridge (1975).
24. D. Y. PARPIA, *J. Mater Sci.* **12** (1977) 844.
25. W. J. SPENCER, "Physical Acoustics", (Academic Press, New York and London, 1968) p. 111.
26. R. D. MINDLIN, *Q. Appl. Math.* **19** (1961) 51.
27. U. K. BONSE and E. KAPPLER, *Naturforsch.* **13a** (1958) 348.
28. U. K. BONSE, "Direct Observations of Imperfections in Crystals" (Interscience, New York, 1962) p. 431.
29. U. K. BONSE, M. HART and J. B. NEWKIRK, "Advances in X-ray Analysis", Vol. 10 (Plenum Press, New York, 1966) p. 1.
30. R. A. YOUNG and C. E. WAGNER, *Brit. J. Appl. Phys.* **17** (1966) 723.
31. K. H. HARUTA, *J. Appl. Phys.* **38** (1967) 3312.
32. A. W. WARNER, *Bell Sys. Tech. J.* **39** (1960) 1193.
33. E. D. FLETCHER, private communication.

Received 28 April and accepted 29 August 1978.